

## Characterisation of Ion Implantation-induced Defects in Certain Technologically Important Materials by Positron Annihilation

P.M.G. Nambissan

Saha Institute of Nuclear Physics, 1/AF Bidhannagar, Kolkata-700 064  
E-mail: pmg.nambissan@saha.ac.in

### ABSTRACT

The application of positron annihilation spectroscopy for the studies of defects produced by different types of charged particles and ions in a variety of materials is discussed with specific examples. The ability to detect and quantify the information through the characteristic parameters of the annihilation radiation in a totally non-destructive method has made the fundamental process of electron-positron annihilation a powerful spectroscopic probe for investigating the structure and properties of materials. Ion implantation produces defects in the structure of solids and the latter can be recovered from the defects by annealing at high temperatures. Here the annealing is done in sequential steps so that the different stages of evolution of defects and their interaction with impurity atoms can be studied systematically. Defects produced by irradiation by particles like protons, alpha, boron and neon ions in materials ranging from simple metals to binary alloys are discussed. A detailed evaluation of the positron lifetimes in terms of the popular positron trapping models is also presented. Further as a special case, the method of extraction of values of several useful physical parameters of inert gas bubbles inside a metal matrix is explained with the help of a model analysis.

**Keywords:** Materials defects, ion implantation, induced defects, strategic materials, special materials, material characterisation, positron annihilation, electron-positron annihilation, defect analysis

### 1. INTRODUCTION

Among the different experimental techniques available for the studies of structural defects in solids, positron annihilation spectroscopy enjoys a unique status. Over the past four decades or more, it has been widely recognised as a highly sensitive and reliable method for the investigation of defects in materials. The foremost advantage of this technique over the other more popular and conventional experimental probes is its non-destructive nature and the ability to provide information on the atomic scale. While x-ray diffraction can give measurable changes only when the defect concentration is high enough and transmission electron microscopy is limited by its resolving power, positrons by virtue of their ability to get trapped even at monovacancies can serve as a powerful tool for the detection and characterisation of such defects and their clusters and monitoring their evolution under controlled changes of experimental variables like temperature, pressure, chemical composition, etc.

The principles that underlie the utilisation of the features of electron-positron annihilation in materials for their defect analysis are rather simple and straightforward. Positron is the antiparticle of the electron, having a unit positive charge and mass same as that of the electron. In a crystalline solid with homogeneous electron density  $n_e$ , the positron can survive for a lifetime given by Dirac's equation<sup>1</sup>

$$\tau_b = (\pi r_0^2 c \xi(r) n_e)^{-1} \quad (1)$$

where  $r_0$  is the classical electron radius,  $c$  the velocity of light and  $\xi(r)$  is the electron density enhancement factor to account for the local increase in density of electrons due to Coulomb attraction by the positron. In metals, for example, it is given as

$$\xi(r) = 1.23r_s + 0.8295r_s^{3/2} - 1.26r_s^2 + 0.3826r_s^{5/2} + 0.167r_s^3 \quad (2)$$

where  $r_s$  is the radius of a fictitious sphere containing one electron. As an example,  $\xi = 2$  for Al.

Vacancy-type defects can trap positrons. In a crystalline solid, the positron starts feeling the repulsion from the atomic nucleus when it tries to approach an occupied lattice site. However, if the lattice site is vacant, the repulsion is nil and the vacancy can act as a deep potential well for the localization and subsequent annihilation of the positron. The absence of the atom also results in a reduced electron density that, according to Eqn (1), would give rise to an enhanced lifetime  $\tau_d$  for positrons annihilating from the defects. Thus a stream of positrons entering into a material containing defects will give rise to a situation governed by the two rate equations

$$\frac{dn_b}{dt} = -\lambda_b n_b - \kappa_d n_b \quad \text{and} \quad \frac{dn_d}{dt} = -\lambda_d n_d + \kappa_d n_b \quad (3)$$

Here,  $\lambda$  stands for the reciprocal of the respective lifetime ( $\tau$ ) and  $\kappa_d$  is the rate of trapping of positrons into the defects. The solution of the above rate equations leads

to an equation of the positron lifetime spectrum as

$$N(t) = \sum_{i=1}^n I_i \exp(-t/\tau_i) \quad (4)$$

where  $n$  stands for the number of lifetimes that can be resolved by fitting the experimental spectrum to the above equation, giving an acceptable variance of fit ( $= 0.90 - 1.15$ , in general).

There are two more basic features of electron-positron annihilation process that can be utilized to extract information regarding vacancy-type defects in solids. These come from the perturbation caused to the electron momentum distribution around the defects that the annihilation signals can reflect in measurable form. When the annihilation of a positron takes place with an electron, their rest masses are converted into energy, which are emitted in the form of gamma ray photons. (The authors rule out the emission as a single quantum of energy, as such a possibility exists only within the nuclear field where the recoil of the nucleus will account for the backward momentum caused by the emission.) The conservation of the linear momentum and energy demands that the two photons, each with an energy equal to the rest mass equivalent of either the electron or the positron (511 keV), should move in exactly opposite directions. However the positron, normally emitted from a radioactive source with a high kinetic energy, will lose the same to the material in which it enters via elastic collisions with the electrons and other energy dissipating process like ionization and electron-hole pair creation, etc. Only the electron will therefore have a momentum strong enough to influence the momentum and energy of the emitted photons. The result is that the two gamma rays will deviate from anticollinearity through a certain angle  $q$  that is related to the electron momentum  $p_z$  as

$$\theta = p_z / m_0 c \quad (5)$$

Thus the coincident counts collected at different angles for a fixed interval of time at each will represent the electron momentum distribution profile across the Fermi momentum and is a very accurate method of determining the electronic structure of many material systems<sup>1</sup>. Besides this, the same non-zero linear momentum of the annihilation electron will impart a Doppler shift in the energy of the gamma rays. Its magnitude depends on the projection of the electron momentum in the direction of detection of the gamma ray and is given by

$$\Delta E = p_x c/2 \quad (6)$$

Thus the energy spectrum of the annihilation gamma rays is also able to reflect the electron momentum distribution in the solid, although it is limited in accuracy by the resolution of the detector being used. Nevertheless, in following the systematic variation against a certain experimental variable qualitatively, the Doppler broadening of the gamma ray energy spectrum is good enough to provide qualitative changes that can be monitored.

In this paper, a few case studies in which the use of

positron annihilation has been made with a high degree of success has been highlighted to monitor the production of defects by ion-irradiation in metals and alloys and their evolution under isochronal and isothermal heat treatments of the irradiated material. The irradiation by energetic ions is both a very efficient method and a possible catastrophe resulting into the production of rich concentrations of defects in materials. From the technological side, it has a special importance as it is highly essential to know about the radiation resistance capability of structural materials to be used for fabrication of nuclear reactor components. The defect evolution processes under such annealing sequences generally involve the migration and agglomeration of smaller vacancies into larger clusters, further coarsening leading to the formation of voids, interaction of impurity atoms with the vacancies and transformation of voids into gas-filled cavities, normally termed as bubbles. We shall discuss about them in detail in the following sections.

## 2. EXPERIMENTAL

Irradiation of the material under interest is normally carried out in a particle accelerator, like the cyclotron at the Variable Energy Cyclotron Centre (VECC), Kolkata, or the 14 UD Pelletron at Tata Institute of Fundamental Research (TIFR), Mumbai. The energy of the particles and the total dose of irradiation are chosen based on the range of penetration of the said particles in the material and the approximate defect concentration that is expected. It also depends on the realistic experimental conditions such as the available beam currents and reasonable time of irradiation. Table 1 gives the values of some of these quantities used in the experiments discussed here.

In some experiments, either the energy of irradiation or the thickness of the target material is so chosen that the bombarding particles fully penetrate through the material and escape, leaving trails of defects in their trajectories. Thus the particles themselves do not have any roles in any of the subsequent annealing experiments. If the thickness of the target is larger than the range of penetration of the bombarding ions, they are captured at the end of their trajectories within the material. Depending on the energy required for their migration, these particles may diffuse into the region of defects at certain elevated temperatures. In yet another arrangement, particles of a distribution of discrete energies are implanted in the volume of the material with the specific purpose to study their interaction with the defects they themselves generated. We shall discuss about some such experiments belonging to this category. Here, the so-called variable energy irradiation is achieved by successively degrading the energy of a fixed energy beam from the accelerator using energy absorber foils of different thicknesses that are introduced in the beam path using a rotating wheel with windows covered by these foils at its circumferential border (Fig. 1). High current irradiation often tends to heat the target and some of the defect interaction processes may take place online, leaving no further scope for scrutiny and observation. Hence, the

**Table 1. Energies and doses of particles used in the irradiation experiments**

Expt. No.	Material	Particle	Energy (MeV)	Range ( $\mu\text{m}$ )	Dose (particles / $\text{cm}^{-2}$ )	Reference
1.	<i>W</i>	$\text{He}^{2+}$	32	125	$4 \times 10^{17}$	2
2.	<i>Zr-1.0%Nb</i> <i>-1.0%Sn-0.1%Fe</i>	proton	15	720	$5 \times 10^{21}$	3
3.	<i>Mo</i>	$\text{He}^{2+}$	40	243	$1.4 \times 10^{18}$	4
4.	<i>Al</i>	$\text{He}^{2+}$	0-45	700	$1 \times 10^{18}$	5
5.	<i>Cu</i>	$\text{Ne}^{8+}$	9-145	36	$1 \times 10^{16}$	6
6.	<i>Si</i>	$\text{B}^{4+}$ , $\text{B}^{5+}$	25-72	160	$6 \times 10^{16}$	7
7.	<i>Fe<sub>72</sub>Al<sub>28</sub></i>	$\text{B}^{5+}$	72	70	$1.6 \times 10^{16}$	8

target is always cooled by circulating water through the rear side (Fig. 1). In positron annihilation experiments, the methodology of investigation is based on the detection of gamma rays and hence no stray radioactivity should interfere with the measurements. Sufficient time (days, months and, in some cases, years) therefore needs to be allowed for the irradiated material to cool down the irradiation-induced radioactivity before starting the experiments.

A continuous source of positrons is the primary requirement for the experiments. It should have a convenient half-life so that the measurements are not hampered as a result of fast decay of the source.  $^{22}\text{Na}$  is the most widely used among all the  $\beta^+$ -decaying isotopes as it also emits a 1.28 MeV gamma ray almost simultaneously with the emission of the positron. This is very useful in the measurement of the lifetime of the positron, as we need a birth signal to denote the instant of emission of the positron from the source.  $^{22}\text{Na}$  has a half-life of just 2.7 years, neither too long to limit the availability of positrons, nor too short to abruptly cease it. The annihilation will result in the emission of two 511 keV gamma rays and the detection

of one of them will yield the death signal for the positron. The gamma rays are detected using fast  $\text{BaF}_2$  scintillators coupled with XP2020Q photomultiplier tubes with quartz end-windows to transmit the ultraviolet photons. A time-to-pulse-height converter in a slow-fast gamma-gamma ray coincidence setup generates the pulse with proportionate amplitude and the correlated events are recorded in a multichannel analyser<sup>1</sup>. The side channels employing properly set amplifiers and single channel analysers ensure that only genuine positron lifetime events are ultimately recorded and stored. The “positron lifetime spectra” are then analysed using the universally accepted computer code called PALSfit<sup>9</sup>. The analysis involves the subtraction of the spectral background coming from random coincidence events, deconvolution of the instrumental resolution (full-width at half the maximum = 200 ps) and a correction for the positrons annihilating within the  $^{22}\text{Na}$  source and the thin ( $\sim 2 \text{ mg cm}^{-2}$ ) *Ni* foil that backs and covers it. The resultant spectra are then fitted with Eqn (4) to obtain the positron lifetimes and their relative intensities.

The source is kept sandwiched between two identical disc-shaped specimens of the sample and the positrons are captured and annihilated within the sample. Since the gamma rays are emitted in all directions, a high pure germanium detector of good energy resolution ( $\sim 1.14 \text{ keV}$  at 511 keV) can be kept in another direction to record the Doppler broadened spectrum. The spectral features are generally described in terms of certain parameters derived from its shape and are used for monitoring the changes taking place in the material. The most popular among these is the sharpness of the spectrum, normally denoted as *S* and defined as the ratio of the area falling under the energy segment  $511 \pm 0.64 \text{ keV}$  to the total area under the spectrum ( $511 \pm 8 \text{ keV}$ ). According to Eqn (6), the magnitude of the Doppler shift is proportional to the electron momentum and hence the *S* parameter signifies the fraction of low momentum electrons annihilated by the positrons. Defined as this, it is very sensitive to the annihilation of positrons within the defects as there is a significantly reduced probability for annihilation with the high momentum core electrons of the missing atoms<sup>1</sup>. In metals and alloys, which are the

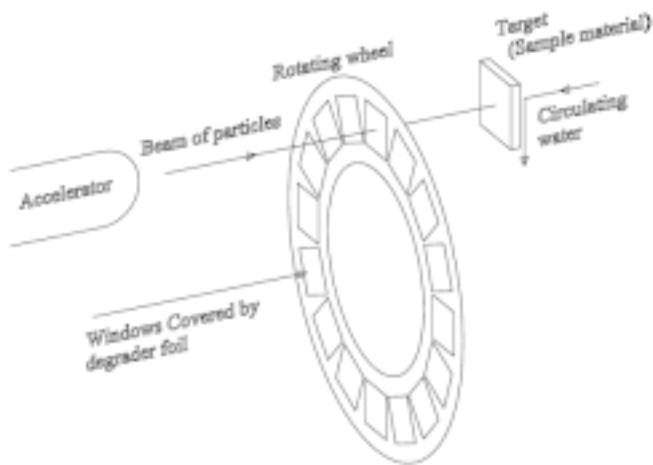


**Figure 1. Schematic diagram of the experimental arrangement used for irradiating the target with particles of differently degraded energies.**

materials covered in this article, the formation of a metastable bound state of positron with electron, known as positronium, can be ruled out owing to the rich density of electrons prevailing throughout, notwithstanding the relative reduction at the vacancy type defects. More discussion on this topic can be seen in popular review articles on the subject of positron annihilation spectroscopy<sup>1,10,11</sup>.

### 3. RESULTS AND DISCUSSION

This Section, briefly reviews the important findings observed in a few chosen original research studies and focus on those aspects that bring to light the versatility of positron annihilation as a powerful defect spectroscopic tool.

#### 3.1 Alpha-Irradiated Tungsten

Tungsten being a metal of great technological importance in the avenue of reactor component design and fabrication, it was thought worth investigating its radiation resistance capability beforehand. High purity (~99.9 per cent) polycrystalline samples were bombarded by 32 MeV alpha particles to a total dose of  $4 \times 10^{17}$  cm<sup>-2</sup>. After the decay of the stray isotopes produced as a result of nuclear transmutation reactions at the time of irradiation, positron lifetime and Doppler broadening measurements were carried out following isochronal annealing of the sample at different temperatures from 100 °C to 1050 °C at intervals of 50 °C. The annealings were done in a vacuum furnace and the samples were cooled to room temperature in vacuum itself to avoid surface contamination and quenching effects. Positron annihilation measurements were performed at room temperature.

In Fig. 2, the variation of the  $S$  parameter as a result of the annealing at different temperatures is illustrated. The dotted line in the figure represents the value of  $S$  for the reference specimens.  $S$  remains constant upto 200 °C showing that no significant processes are taking place in the specimens in this region of temperature. The irradiation resulted in the production of isolated small vacancies in the metal. It is likely that the atoms of impurities present in the specimens were strongly bound to these lower order defects and concealed the recovery of the latter at lower temperatures. At 250 °C, a rise in  $S$  is observed. From our understanding of the defect kinetics in metals, such a behaviour of  $S$  is usually attributed to vacancy migration and formation of vacancy clusters. But this argument contradicts the earlier observations in quenched or proton irradiation studies in tungsten. There existed strong evidences which suggested that vacancies were practically immobile in tungsten at the lower stages of the recovery process<sup>12</sup>. Therefore, the rise in  $S$  at 250 °C is explained on the basis of the dissociation of vacancy-impurity complexes whereby high concentrations of vacancies are released inside the specimens. The fall in  $S$  at 400 °C followed by a rise at 500 °C can be due to the annealing of point defects such as vacancies and the formation of vacancy clusters, in agreement with earlier observations by others<sup>13-14</sup>. However, these clusters appear to be quite unstable as they quickly undergo annealing

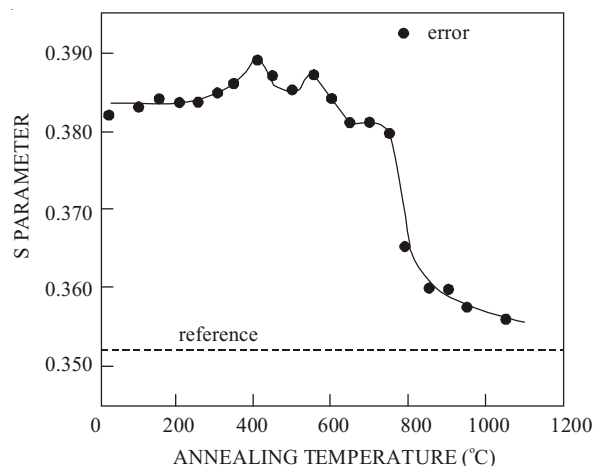


**Figure 2. The variation of the Doppler broadening line shape parameter  $S$  vs isochronal annealing temperature for alpha-irradiated tungsten.**

leading to the formation of bigger size clusters like vacancy loops or microvoids. This process is shown by a fall in  $S$  from 550 °C to 650 °C. These higher order defects are found to be stable over a small range of temperature, i.e., till about 700 °C. Beyond this,  $S$  falls sharply. This is due to the annealing out of the vacancy loops and microvoids. At 1050 °C, which is the highest annealing temperature used in this experiment, the value of  $S$  is still slightly higher than the reference value, which shows that the defect recovery is not yet complete even at this temperature. More details of this work, especially those from the positron lifetime measurements, can be found in the papers published elsewhere<sup>2,15</sup>.

This study and a large number of similar works carried out on simple ion-irradiated metals and alloys had been topics of immense pursuit using positron annihilation during 1970s, 80s and even in the first-half of 90s. Such studies demonstrated the reliability of this technique as a powerful probe for studying ion beam irradiation effects in solids. It should be noted that the range of penetration of positrons of the maximum energy (~545 keV) from <sup>22</sup>Na in materials will be typically a few hundred microns. If the implantation profile of the particles extends beyond this range, all positrons will be annihilating from the region of radiation damage. On the contrary, if the particles could traverse only to small depths and the energetic positrons make their way to depths beyond, the spectrum will be dominated by events from the undamaged region and hence the required information about the defects will be partially lost. This is a problem often encountered in heavy ion irradiated solids (See later sections). A solution to this problem is the use of low energy positron beams, which are nowadays very popular. For a detailed review of the applications of slow positron beams<sup>16</sup>.

#### 3.2 Proton-irradiated Zirconium Alloy

From a simple metallic system like tungsten, we now move over to a sophisticated metallic alloy system consisting

of zirconium and three other elements in trace amounts. This particular alloy, popularly known as zirlo, contains 1.0 per cent *Nb*, 1.0 per cent *Sn* and 0.1 per cent *Fe* besides the basic *Zr* matrix. It is a widely accepted structural material used for constructing several components in nuclear reactors and power plants. In such devices, there is possibility of exposure of such components to powerful radiation and high temperature. Hence knowledge of evolution of radiation-induced defects under heat-treatment is considered vital by material scientists and technologists. An experiment was performed by irradiating this sample by 15 MeV protons to a dose of  $5 \times 10^{21} \text{ cm}^{-2}$  and the sample was isochronally annealed upto 1023 K. Figure 3 gives the nature of variation of the *S* parameter and Fig. 4 depicts those of the lifetime  $\tau_2$  and intensity  $I_2$ .  $\tau_2$  is the longer of the two lifetimes resolved from the spectra and represent the predominant positron-trapping centre in the irradiated alloy, viz., the vacancy clusters. Its variation with annealing temperature is very useful in understanding how the vacancy clusters are taken through the different stages of evolution towards the recovery of the sample from the defects.

The as-irradiated specimens consisted of defects giving a lifetime  $\tau_2$  in the range from 244 ps to 292 ps for the trapped positrons. If they are of the vacancy-cluster-type, this value should imply that they essentially consist of 2-3 monovacancies each. It is not possible to rule out the presence of other small order defects since the irradiation-induced displacement cascades ultimately are likely to collapse into dislocation/vacancy loops. It is also possible that the into dislocation/vacancy loops. It is also possible that the oxygen atoms present in the octahedral sites of the hexagonal lattice may diffuse in and segregate near these defects at ambient temperatures. (Typical oxygen concentration in this alloy is 900-1300 ppm. This segregation process is usually known as Cottrell effect.) From the behavior of  $\tau_2$  and intensity  $I_2$ , it was found that the annealing is remarkably

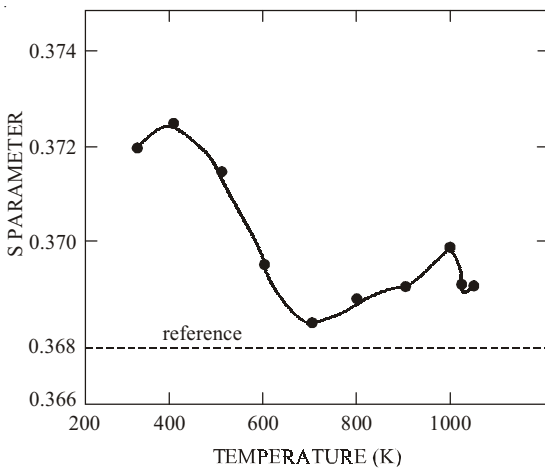


**Figure 3.** The variation in *S* parameter with isochronal annealing temperature of proton-irradiated zirlo. (Reference denotes sample annealed at 1023 K for 4 h prior to irradiation).

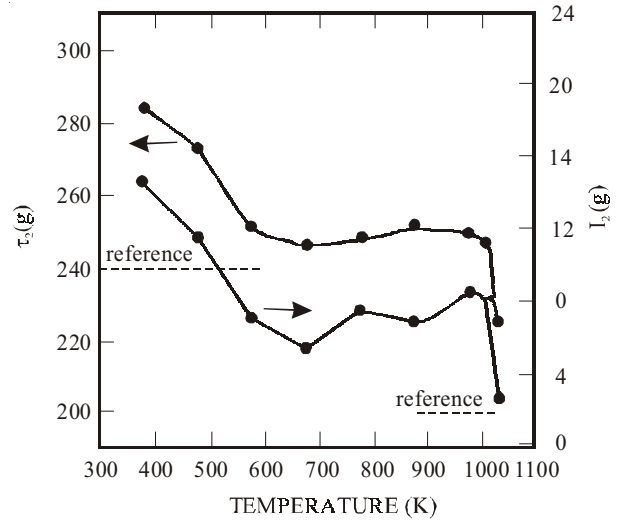


**Figure 4.** The lifetime parameter  $\tau_2$  and intensity  $I_2$  versus annealing temperature in proton-irradiated zirlo. The values for an annealed reference sample are also shown.

sharp and consists of three distinct stages (Fig. 4). Initially both these parameters fall drastically, indicating that there existed a significant number of divacancies or trivacancies in the as-irradiated sample which did not form complexes with the atoms of either the solute elements or the oxygen diffusing out of the octahedral sites. The annealing stage corresponding to the recovery from these defects coincides with that of dislocation/vacancy loops and ends at 673 K. The intermediate stage of defect evolution from 673 K to 973 K involves the release of fresh positron trapping sites into the sample. When we had calculated the positron trapping rate (i.e., the number of positrons trapped per unit time by the entire concentration (*C*) of the defects)  $\kappa_d$  using the equation

$$\kappa_d = \frac{I_2}{I_1} \left( \frac{1}{\tau_b} - \frac{1}{\tau_2} \right) \quad (7)$$

We had observed an increase of it in this temperature range<sup>3</sup>.  $\kappa_d$  depends both on the specific positron trapping rate (*m*) of the kind of defect and its concentration (*C*) through the relation  $\kappa_d = mC$ . While the former has a direct bearing on the positron lifetime trapped in it, the latter will be reflected in the measured intensity  $I_2$ . Fig. 4 shows a sharper increase in the intensity than in the lifetime, which indicates rather the presence of additional trapping centres than a characteristic defect evolution stage. The release of vacancies at this temperature is possible if the solute atom-vacancy complexes start to dissociate. The sharp fall of the parameters above 973 K finally completes the defect recovery processes in the  $\alpha$ -phase. A small value ( $\sim 3\%$ ) of  $I_2$  survives the isochronal annealing upto 1023 K, showing that the annealing of defects is still not complete. As the  $\alpha \rightarrow \beta$  phase transition was imminent to occur above this temperature, further investigation needs complementary support from alternative experimental studies. The results, however, give strong evidence for the instant modification

of defect microstructures produced in zirlo due to proton-irradiation by the substitutional solute atoms which considerably interact with the irradiation-induced vacancies to form solute atom-vacancy complexes. Also, the oxygen atoms appear to prevent the remaining vacancies from agglomerating into voids, and instead, only divacancies and trivacancies are formed. The annealing characteristics are not adversely affected either by the impurities or their complexes with vacancies<sup>3,17</sup>.

### 3.3 Helium-implanted Molybdenum

The advent of the discovery of formation of gas-filled cavities (or more popularly called bubbles) in inert gas ion-implanted solids marked the beginning of a new line of research using positrons. Low energy inert gas ions, when implanted in a solid, will be left to precipitate in the form of dense platelets within the interstitial planes. But the large vacancy clusters or voids produced by energetic particles will act as nucleation centres for the formation of dense three-dimensional bubbles. The said transformation of large vacancy clusters known as voids into bubbles was a remarkable defect-impurity interaction stage revealed by positron annihilation parameters. The sharp decrease in  $t_2$  observed around 1123 K in Fig. 5 is an example<sup>4</sup>. Identical observations in a number of simple and refractory metals have been reported<sup>18-21</sup>. The bubbles are found stable thereafter despite annealing of the sample at further elevated temperatures.

### 3.4 Solid Bubbles in Aluminum

The studies reported<sup>18-21</sup> revealed a temperature approximately 0.35 the melting temperature of the metal to activate the helium atoms to migrate and fill the empty voids. Since refractory metals have very high melting points (> 2000 K), it was rather difficult to follow the growth stage of the bubbles at high temperatures. It was therefore thought prudent to imitate the system in a metal with relatively low melting temperature so that the bubble growth processes can be monitored and qualitatively extrapolated to metals melting at high temperatures. Although not technologically called for, aluminum (*Al*) offers as a good choice due to its relatively low (933 K) melting temperature and low induced radioactivity. High energy alpha particles were uniformly implanted (Table 1. and Fig. 1) in *Al* and the sample was isochronally annealed at regular temperatures close upto the melting point. Positron annihilation measurements were done at room temperature after each annealing and cooling. The measured positron annihilation parameters and their variation with the annealing temperatures indicated the formation of helium bubbles at room temperatures and their growth at higher temperatures<sup>21</sup>.

It was found that the lifetime ( $\tau_B$ ) of positrons getting trapped in such bubbles will decrease monotonically with the increase in gas atom density. An empirical relation, known as Jensen-Nieminen relation<sup>22,23</sup>, is used to correlate these two quantities. The relation for the case of helium in *Al* is as given below.

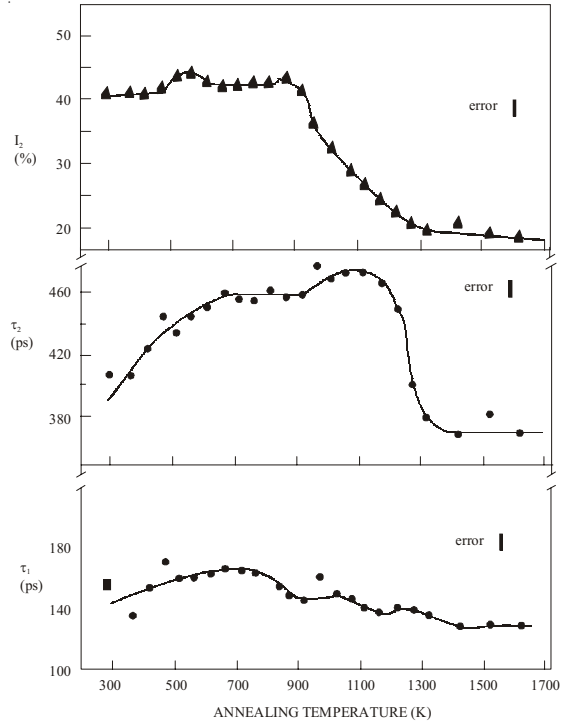


**Figure 5. Variation of the resolved positron lifetime parameters  $\tau_1$ ,  $\tau_2$  and  $I_2$  versus isochronal annealing temperature for molybdenum uniformly implanted with helium to concentration 715 appm (atomic parts per million).**

$$\tau_B \text{ (ps)} = 500 - 2350 n_{He} (\text{\AA}^{-3}) \quad (8)$$

From the values of the lifetime that was obtained in the experiment, the helium atom density obtained is about  $10^{22} \text{ cm}^{-3}$  and is comparable with any metallic atomic density. Hence, a high density equation of state was used<sup>24</sup> to deduce the bubble pressure for fluid helium<sup>24</sup>.

$$P_f = Z n_{He} k_B T \quad (9)$$

where  $k_B$  is the Boltzmann constant. The compressibility factor  $Z = Z(T, T_m, n_{He})$  is evaluated as

$$Z = (1-\rho)(1+\rho-2\rho^2) + (1-\rho)^2 B(T) n_{He} + (3-2\rho)\rho^2 z_1 - 50(1-\rho)\rho^2 \quad (10)$$

Here  $z_1 = 0.1225 v_1 T_m^{0.555}$  is the compressibility on freezing,  $\rho = v_1 n_{He}$  is a reduced particle density and  $B(T) = 170 T^{-1/3} - 1750 T^{-1}$  (in  $\text{\AA}^3$ ) is a virial coefficient.

The helium melting temperature  $T_m$  is obtained by solving the equations for the fluid volume per atom upon melting<sup>24,25</sup>

$$v_1 = 56 T_m^{-0.25} \exp(-0.145 T_m^{0.25}) \quad (11)$$

$$\text{and } v_1 = 1/n_{He} + \Delta V_m / N_A \quad (12)$$

is the Clausius-Clapeyron equation.

$$\text{Here } \Delta V_m (\text{\AA}^3) = 0.6640 (P_m + 1.604)^{-0.3569} \quad (13)$$

$$\text{and } P_m (\text{GPa}) = 0.001691 T_m^{1.555} - 0.0008112 \quad (14)$$

The total input helium concentration  $N_{He}$  can be obtained from the implantation parameters by knowing the cross

sectional area of the alpha particle beam falling on the metal and the range of penetration of the alpha particles in it. If no implanted helium escapes the sample, which is likely the case as the ions are implanted upto considerable depths in the metal, consistency demands that  $N_{He}$  should also equal the total number of atoms in the entire number of bubbles present in unit volume of the metal. Thus

$$N_{He} = C_B(4\pi/3)r_B^3 n_{He} \quad (15)$$

which can be recast into a quadratic equation

$$(H/A) r_B^2 + (H/B) r_B - 1 = 0 \quad (16)$$

The two constants are  $A = 9.07E15 \text{ \AA}^{-1}\text{s}^{-1}$  and  $B = 3.30 E14 \text{ \AA}^{-2}\text{s}^{-1}$  and  $H = (4\pi n_{He} \kappa B)/(3S_f N_{He})$ . The scaling factor  $S_f$  accounts for the dependence of the trapping efficiency on the density of helium atoms<sup>22,23</sup>.

If the bubble pressure equals the internal surface free energy of the metal cavity housing it, the bubble is said to be in equilibrium. In such cases, it can be shown that

$$P_{eq} = 2\gamma/r_B \quad (17)$$

where  $\gamma (= 1 \text{ Nm}^{-1})$  is the surface tension of the metal. By comparing the pressure from Eqn (9) with that obtained using the value of  $r_B$  of Eqn (16) in Eqn (17), the state of the bubble, i.e., underpressurised, in equilibrium or overpressurised, can be predicted.  $P_f = 7.7 \text{ GPa}$  from Eqn (9) and  $P_{eq} = 0.1 \text{ GPa}$  from Eqn (17). The bubbles are thus highly overpressurised.

Equation (14) is in fact identical to the well-known Simon-Glatzel equation, which connects the melting temperature  $T_m$  with the corresponding pressure  $P_m$ , and is given by

$$P_m \text{ (GPa)} = A [(T_m/T_0)^c - 1] \quad (18)$$

where  $A = 0.0051 \text{ GPa}$  and  $c = 1.5602$  are constants and  $T_0 = 2.045 \text{ K}$  for He. Under normal atmospheric pressure, He attains the liquid phase at 4.2 K and the reported freezing temperature is 2 K. In the present case of highly overpressurized He bubbles, positron lifetimes were measured *in-situ* at temperatures from 20 K to 300 K. The  $P_f$  (Eqn (9)) vs.  $T$  curve for fluid helium is found to intersect the Simon-Glatzel curve at about 190 K (Fig. 6). This indicates that, as the temperature is lowered, the overpressurised bubbles transform to the solid phase and the pressure inside the bubbles should be recalculated using a high density equation of state for solid bubbles.

The first task is to delineate the effects of thermal lattice contraction of the host metal ( $Al$ , in this case). The procedure adopted by R.M. de la Cruz<sup>26</sup>, *et al.* is used. The positron lifetime at any temperature ( $T$ ) lower than room temperature (RT) can be written as

$$\tau_T = \tau_{RT} [1 - \gamma \int_{RT}^T \beta(T') d(T')] \quad (19)$$

where  $\tau_{RT}$  is the positron lifetime at room temperature,  $b$  is the volume thermal expansion coefficient. The volume coefficient of the bulk positron lifetime  $g$  is given by

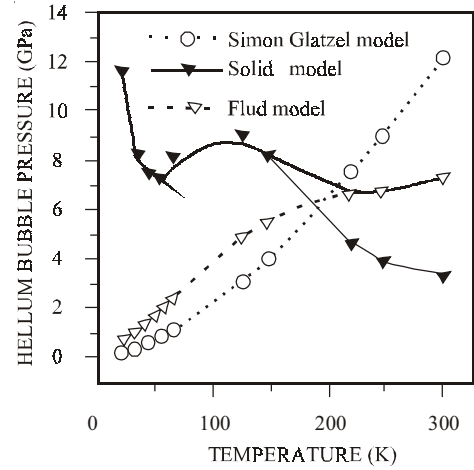


**Figure 6.** The calculated helium bubble pressure at various sample temperatures. The open triangles denote the pressure obtained from the fluid bubble model and closed triangles those from the solid bubble model. The Simon-Glatzel equation for the freezing of helium is shown by the dashed line. The solid line is drawn to guide the eyes through the actual state of the bubbles, i.e., fluid at  $T > 190 \text{ K}$  and solid at  $T < 190 \text{ K}$ .

$$\gamma = + \frac{V}{\tau} \left( \frac{\partial \tau}{\partial V} \right)_p = - \frac{V}{\lambda} \left( \frac{\partial \lambda}{\partial V} \right)_p \quad (20)$$

where the positron lifetime  $\tau = 1/\lambda$ . A similar expression was also derived for the variation of the  $S$  parameter. The results of the analysis carried out, for example, in a defect-free  $Al$  reference sample are shown in Fig. 7.

To calculate the solid bubble pressure, as described by H. Trinkaus<sup>24</sup>, the free energy is split into a static part and a harmonic part. The static potential energy is calculated using the Beck's potential for the interaction of the He atoms and considering all the neighbor atoms upto a distance of  $10 \text{ \AA}$  in an fcc structure. The Beck's potential used here has the form (for  $k \leq 13$ )

$$\phi(r_k) = 398.7 \exp(-4.93 k^{1/2} n_{He}^{-1/3} - 7.485 \times 10^{-4} k^3 n_{He}^{-2}) - 0.435 (k n_{He}^{-2/3} + 0.362)^{-3} [1 + 3.236 (k n_{He}^{-2/3} + 0.362)^{-1}] \quad (21)$$

and is schematically shown in Fig. 8. For the  $k^{\text{th}}$  nearest atom in an fcc lattice,  $r_k = (k/2)^{1/2} a$ , where  $a$  is the lattice constant. For  $k > 13$ ,  $r_k = (k/2 + 1)^{1/2} a$  and the numerical coefficients in Eqn (21) will change accordingly.

The static lattice pressure of the solid bubble is estimated from

$$P_0 = - \frac{1}{2} \sum_k N_k \frac{d\phi(r_k)}{dv} \quad (22)$$

where  $v = 1/n_{He}$  is the volume per atom.  $N_k$  is the number of  $k^{\text{th}}$  neighbour atoms at a distance  $r_k$  from a given atom. The harmonic energy is given by

$$E_h^* = 3k_B T [1 + (1/12) (\theta_E^* / T)^2] \quad (23)$$

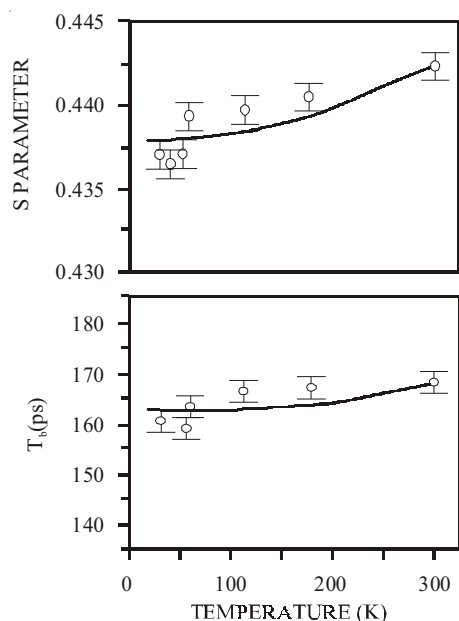


Figure 7. Change in *S* parameter and positron lifetime  $\tau_b$  in a pure unirradiated Al sample with lowering of temperature. The lines denote a fit carried out following the procedure given by de la Cruz, *et al*<sup>26</sup>.

The effective Einstein temperature in the above equation is obtained from

$$\theta_E^* = 11,800 n_{He}^{1/2} \exp(-0.8 n_{He}^{-1/2}) \quad (24)$$

The contribution of this energy to the helium bubble pressure is

$$P_h = (0.5 + 0.4 n_{He}^{-1/2}) n_{He} E_h^* \quad (25)$$

The total bubble pressure  $P_s = P_0 + P_h$  of the solid bubble thus calculated is plotted against temperature and is also shown in Fig. 6. It is interesting to note that the solid pressure curve intersects the fluid pressure curve at the same point through which the Simon-Glatzel curve passes through and is a vivid indication to the fact that below this temperature (i.e., ~190 K), the bubble is indeed in a solid phase<sup>5</sup>.

Further to verify the solidification of the bubbles, was

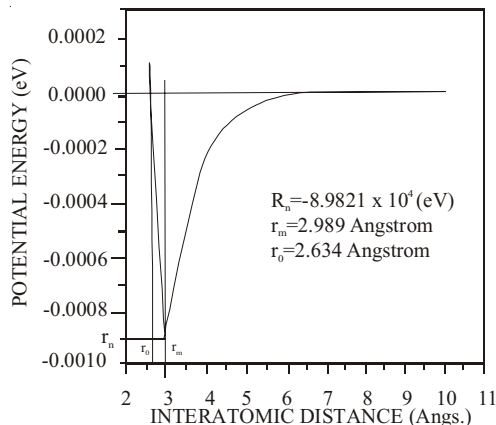


Figure 8. The form of the Beck's potential representing the interaction between two helium atoms.

calculated the ultrasonic transverse velocity of propagation through solid helium<sup>25</sup>

$$u_t = (\theta_D k_B / \hbar) (17/144 p^2 n_{He})^{1/3} \quad (26)$$

where the Debye temperature

$$\theta_D = 17.76 T_m^{0.6219} \quad (27)$$

The ultrasonic velocity  $u_t$  thus obtained for different temperatures below 190 K is plotted against the corresponding bubble pressure  $P_s$  and is shown in Fig. 9. It can be fitted with the relation

$$u_t = a P_s^b \quad (28)$$

The value of  $b$  obtained is 0.08 whereas Mills<sup>25</sup> *et al.* had obtained  $b = 0.33$ . The difference is due to the isothermal variation used by Mills<sup>25</sup>, *et al.* whereas the pressures obtained at different *in-situ* temperatures have been used by the author Nevertheless, that such a relationship holds good is an indication to the solidified phase of the helium bubbles at these temperatures.

### 3.5 NEON-IMPLANTED COPPER

The studies of defects produced by heavy ions in solids using the conventional methods of positron annihilation spectroscopy have one serious disadvantage, as was stated before. The ions have relatively less ranges of penetration compared to protons or alpha particles. The positrons, on the other hand, have high kinetic energy when emitted from the <sup>22</sup>Na source and hence will traverse larger depths and majority of them will annihilate in regions free of the radiation-induced defects and damage. In other words, the fraction of positrons annihilating from the defect region will be relatively small and hence low energy positron beams are the apt solution. Still, to some extent, the same method can be used if only one is interested in extracting qualitative information rather than attempting to infer anything quantitative. Such works are also reported and we shall discuss a few such cases here. The extension of the studies mentioned earlier for helium to heavier inert gases was in the offing and we have performed experiments using neon. In this case, copper (Cu) was chosen as the material since

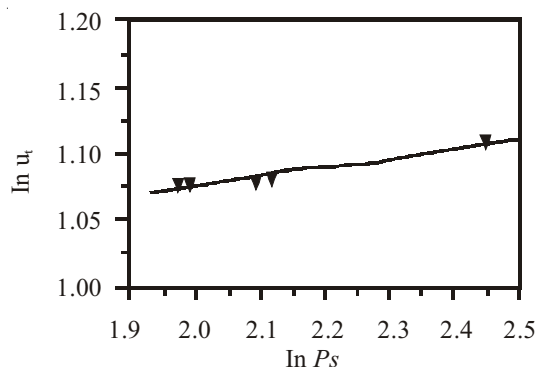


Figure 9. The variation of the ultrasonic transverse velocity component at different pressures of the solid helium bubbles.

it has also a got a relatively low melting temperature (1356 K) and so the defect evolution and defect-gas interaction stages can be brought under investigation within the framework of realistic experimental conditions.

The implantation parameters are given in Table 1. As usual in the case of ion-irradiated metals, we obtained two positron lifetimes  $t_1$  and  $t_2$  with intensities  $I_1$  and  $I_2$ . In order to understand the different defect evolution stages, we first calculated the expected values of the shorter lifetime  $t_1$  using the two-state and the three-state trapping models. In the former case, the solution of eqn (3) gives the following relation.

$$\frac{1}{\tau_1} = \frac{1}{\tau_b} + \kappa_d \quad (29)$$

in which the trapping rate  $\kappa_d$  is calculated using Eqn (7). Although the said model held good in the final stages of defect evolution, the initial defect recovery stages implied the presence of one more prominent defect species that trapped the positrons. Hence  $\tau_1$  was recalculated using the three-state trapping model Eqn given by

$$\tau_1^{cal} = \frac{1 + \frac{\kappa_1}{\lambda_1} \left( 1 + \frac{\kappa_2}{\lambda_b - \lambda_2 + \kappa_1} \right)}{\lambda_b + \kappa_1 + \kappa_2} \quad (30)$$

where the annihilation rate  $\lambda = \tau^{-1}$  in the respective cases and the trapping rates have the form

$$\kappa_1 = \frac{\tau_1(\lambda_b - I_2\lambda_2) - I_1}{\tau_d - \tau_1} \quad (31)$$

$$\kappa_2 = \frac{I_2}{I_1}(\lambda_b - \lambda_2 + \kappa_1)$$

The results are as shown in Fig. 10. In the initial stage upto 623 K, a three-state trapping model implying two different types of defects seems to be more feasible. Above this temperature, both the models converge to indicate that one of the two types of defects has annealed out. The experimental values are consistent with those predicted by the trapping models above 623 K.

The calculated positron trapping rates versus the annealing temperature curve, shown in Fig. 11, gives interesting results. One of the trapping rates predicted by the three-state trapping model vanishes by 623 K, indicating the gradual but complete annealing of lower order defects like monovacancies, dislocation loops, etc. created within the sample due to implantation by the energetic ions. Above this temperature, the trapping rate for the higher order defects only persist, and is also in agreement with the two-state model trapping rate<sup>6</sup>.

The dislocations, loops and monovacancies anneal out during the heat treatment at temperatures upto 623K. At the same time, the implanted neon atoms would move into the large size voids created by the implantation and transform them into bubbles. This process drastically decreased the positron lifetime  $\tau_2$  due to the increased electron density brought in by the neon atoms. Above 623K,  $t_2$  increases

and  $I_2$  decreases in accordance with the expected bubble growth (Fig. 12). The growth takes place by migration and coalescence. The growth continued upto the highest annealing temperature used (1273 K). Since the intensity  $I_2$  did not vanish, it means that the bubbles remain within the sample and are stabilized. However, some of the bubbles near the surface of the samples seemed to have burst out and escaped from the sample, since the samples were found to exhibit ruptures on its surfaces after annealing at the highest temperatures (1273 K).

### 3.6 BORON-IMPLANTED SILICON

The results of studies on a particular material subjected to even the same irradiation and post-irradiation heat treatment and even using the same experimental probe may be sometimes given contradicting interpretations by different research groups and hence additional confirmation may be required by improving the rightness of the experimental procedure and precision and accuracy of the measurements. Due to the ever-increasing potential in areas of semiconductor science and technology, silicon (Si) continued to evoke interests in researchers and implantation of different kinds of ions to explore structural modification and changes in properties is a hot area of research. However, controversies

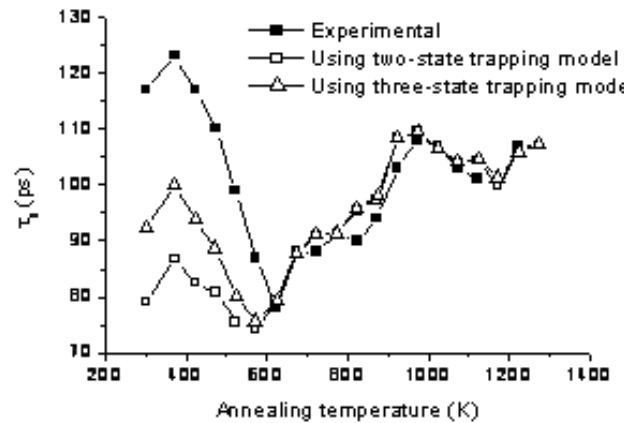


Figure 10. The variation of the calculated shorter lifetime  $\tau_1$ —two state and three state trapping model based—and the experimentally measured  $\tau_1$  with isochronal annealing temperature in neon-implanted copper.

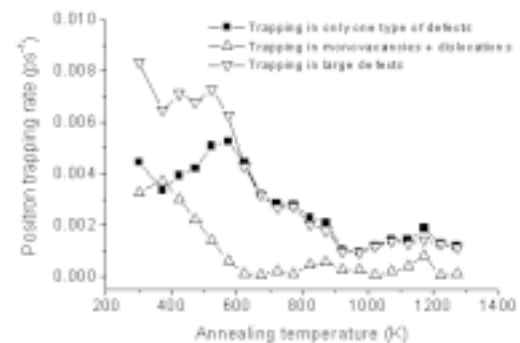
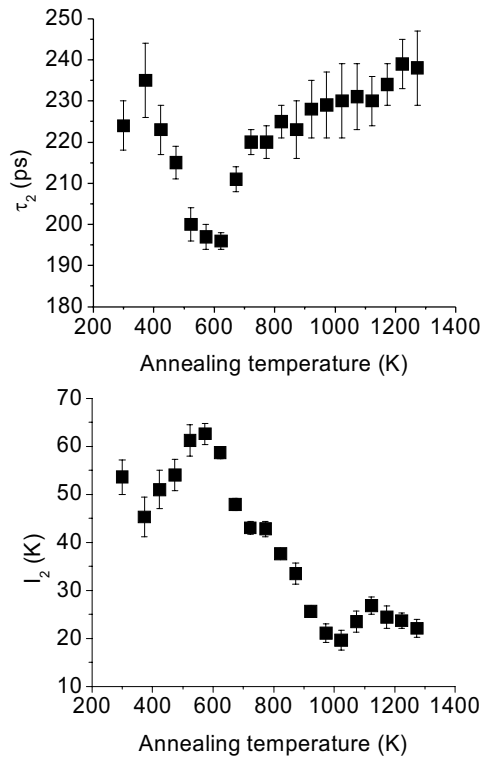


Figure 11. The variation of the positron trapping rates with isochronal annealing temperature in neon implanted copper.



**Figure 12.** The variation of the lifetime  $\tau_2$  and relative intensity  $I_2$  with isochronal annealing temperature in neon implanted copper.

sometimes erupted due to conflicting observations and additional experimental evidences were sought to reach at the right conclusion. The question of thermal vacancy generation at temperatures above  $0.65 T_m$  common in most metals was elusive in the case of Si for some time<sup>27</sup> and an explanation was presented in terms of the interaction with hidden impurities by some other research groups<sup>28</sup>. The present investigation was, therefore, undertaken basically to answer this question. The isochronal annealing behavior of the positron lifetimes and the intensity  $I_2$  is shown in Fig. 13. The observations can be interpreted as follows. Positrons predominantly annihilated with electrons of silicon and the boron atoms practically did not influence the positron annihilation characteristics at the initial stages of annealing of the irradiation induced defects. The temperature of annealing of divacancies (above 573 K) agreed with the results reported in literature. The most important defect-evolution stage is observed above the annealing temperature of 873 K when the positron annihilation characteristics drastically deviated from the ongoing trends (Fig. 13). Here the implanted boron atoms further diffused beyond the range of their initial penetration ( $\sim 160 \mu\text{m}$ ) and decorated the vacancies, presumably generated by thermal effects. While the irradiation-induced defects fully annealed out of the sample, the boron atoms have diffused and redistributed uniformly throughout the sample as in the case before the irradiation. This again proves that processes like thermal vacancy generation can aid the diffusion of the atoms beyond the implantation depth<sup>7</sup> and the said stage could have been suppressed had impurity atoms other than the implanted boron been present.

It underlines the need to choose samples with the utmost available purity for application purposes.

### 3.7 Boron-irradiated $Fe_{72}Al_{28}$ alloy

As the last example in this paper, we discuss the findings from a recent experiment on boron-irradiated (Table 1)  $Fe_{72}Al_{28}$  alloy and the different processes involved in the defect-recovery of the sample.  $Fe_{72}Al_{28}$  is a binary system which crystallises in the BCC structure with two interpenetrating sublattices  $A$  and  $B$ . The atomic arrangements can be in any one of the three possible ways –  $DO_3$ ,  $B2$  and  $\alpha$ . In the  $DO_3$  structure, the iron atoms occupy the  $A$ -sites and iron and aluminium atoms take alternate positions in the  $B$ -sublattice. The  $B2$  structure is with the  $A$ -sites fully occupied by iron atoms and iron and aluminium atoms randomly distributed in the  $B$ -sublattice. The  $\alpha$ -structure is characterised by a total random distribution of iron and aluminium atoms at all possible sites, irrespective of  $A$  or  $B$ . Particle irradiation will induce vacancies in the structure and the role vacancies could play in controlling the defect dynamics and inter-sublattice atomic redistribution had been a subject of intense debate. Positron annihilation being a reliable and sensitive defect spectroscopic probe was expected to be very useful in studying these aspects

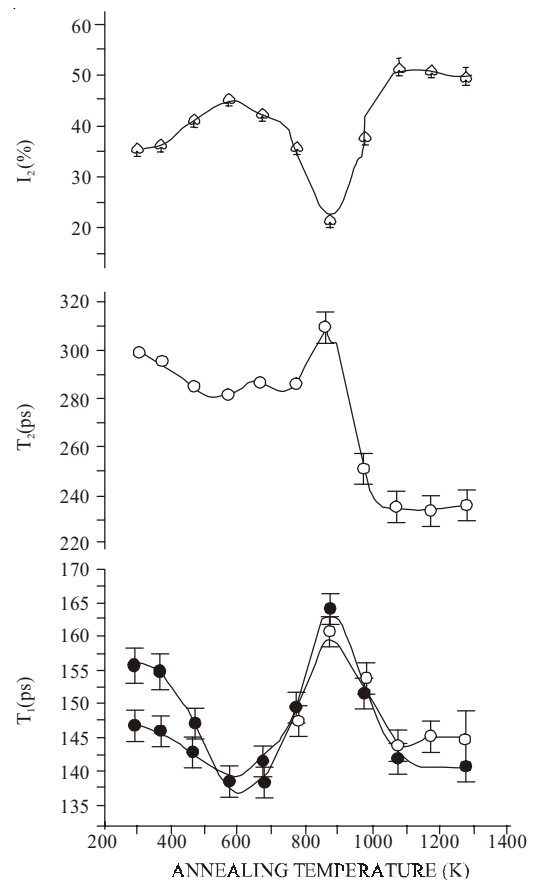


**Figure 13.** The two positron lifetimes  $\tau_1$  and  $\tau_2$  and the relative intensity  $I_2$  versus isochronal annealing temperature in boron-implanted Si. The open diamond symbols indicate the values of  $\tau_1$  obtained from the two-state trapping model.

in more depth, especially since vacancies have been introduced in the present samples by ion irradiation. The use of the highest available beam energy (72 MeV) made the irradiation-induced damage distribute upto 70 mm deep from the irradiated surface, whereas the positrons from the  $^{22}\text{Na}$  source have a maximum penetration depth of 280 mm. Using the mass absorption coefficient for positrons in the alloy ( $\sim 0.022 \mu\text{m}^{-1}$ ), it could be estimated that 71% positrons annihilate within the region of defects whereas the rest annihilate in regions not containing any defects.

Since two types of atoms were involved in the structure of the material, it was necessary to identify the atomic sites at which positrons could be trapped and annihilated. For this, we had employed an element-specific defect analytic method called coincidence Doppler broadening measurements and is widely accepted nowadays for accurately determining the chemical environment around the positron trapping sites. The details of this technique are not described here and can be obtained from the original references<sup>29,30</sup>. From the results obtained from these measurements<sup>8</sup> and from the measured positron lifetimes, it could be concluded that the unirradiated alloy with the  $\text{DO}_3$  structure itself was characterized by vacancies in the B-sublattice and they grew in size with Al atoms being displaced from the B-sublattice on bombardment with boron. Subsequent transport of the Fe atoms from the A-sublattice to the B-sublattice helped in the partial recovery of these defects while the defects generated as a result in the A-sublattice acted as fresh trapping centers for the positrons. These are evident from the annealing behavior of the positron annihilation parameters depicted in Figs 14 and 15. The alloy went through an order-disorder transition ( $\text{DO}_3$  to  $\alpha$ ) at the time of irradiation itself, implied by a changed bulk positron

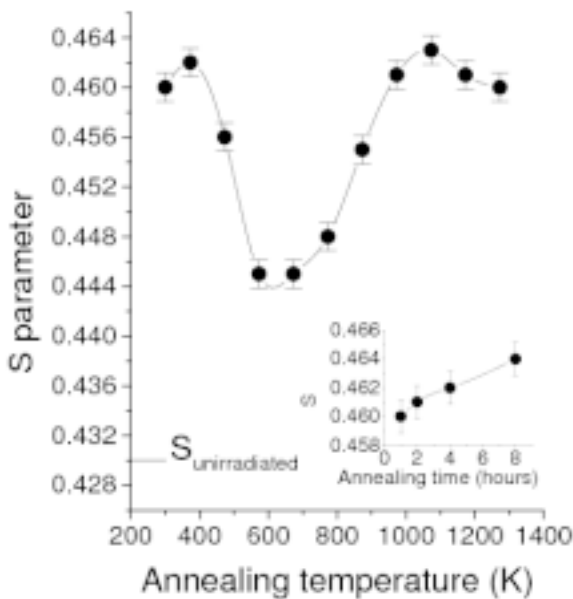


Figure 14. The  $S$  parameter vs the isochronal annealing temperature and (inset) after isothermal annealing at 1273 K for different hours of boron-irradiated  $\text{Fe}_{72}\text{Al}_{28}$ .

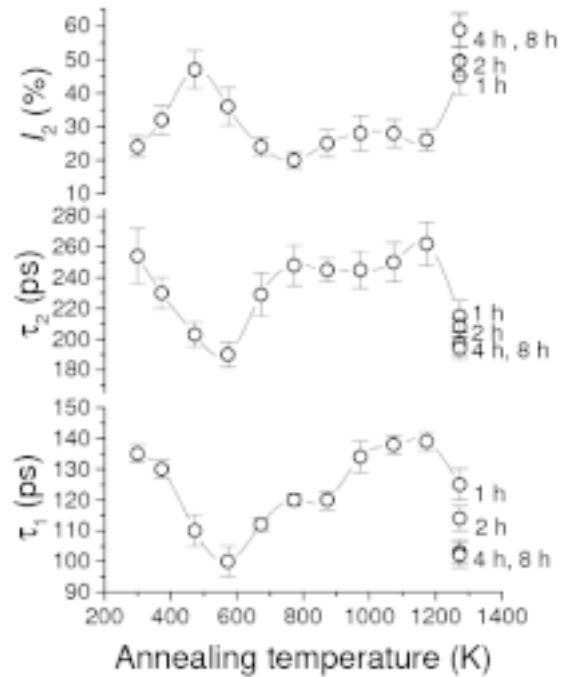


Figure 15. The positron lifetimes  $\tau_1$  and  $\tau_2$  and the relative intensity  $I_2$  vs the isochronal annealing temperature and isothermal annealing time (shown against 1273 K) of boron-irradiated  $\text{Fe}_{72}\text{Al}_{28}$ .

lifetime (113 ps to 153 ps) and isochronal annealing behaviour of the a-phase was not influenced by outside entities like impurities or transmutation products. Rather, the atomic transport and diffusion continued. Positron annihilation parameters went through characteristic changes to depict the occurrence of these processes. The results of the final isothermal annealing at 1273 K bringing in a decrease and leveling off of the positron lifetimes and a saturation of the positron lifetime intensity points to a gradual but partial restoration of the original ordered state and the stabilization of the thermal vacancies by the implanted  $\text{B}^{5+}$  ions<sup>8</sup>.

#### 4. CONCLUSIONS

The aim of the present article is to highlight the utility of electron-positron annihilation spectroscopy for studying ion-irradiation induced structural changes in materials. As mentioned in the introduction, positron annihilation offers a viable experimental technique that is absolutely non-destructive in its application. One salient feature of this technique is its defect-specificity, i.e., sensitive only to vacancy type defects whereas positrons get repelled from the positively charged nuclei of interstitial atoms. All the three basic characteristics of the electron-positron annihilation process, viz., lifetime of the positron, angular correlation of the annihilation radiations and Doppler broadening of the gamma ray spectrum, can be utilized to derive the required information. Since the technique is non-destructive, the same sample can be subjected to different types of treatments like irradiation to different doses, annealing at different temperatures and for different durations and even

variation of the chemical composition. After each treatment, the same measurements can be carried out for comparison and the exercise can be repeated for any number of such treatments. The important findings in the various examples discussed in this article underline the versatility of this nuclear spectroscopic technique that has won its legitimate place in the investigation of problems relevant in condensed matter physics and material science.

It may be added here that there exists vast literature on the subject of use of positron annihilation spectroscopy for the studies of ion-implantation induced defects in solids and reviewing all of them in a single article will render it voluminous and unmanageable. The interested reader may look into review articles on this subject<sup>31-32</sup> and the references therein. A few references are cited at the end<sup>33-40</sup>.

#### ACKNOWLEDGEMENTS

The author expresses deep sense of gratitude to his numerous collaborators who had been part of the experiments discussed in this paper. Especially the operating staffs of the cyclotron at VECC, Kolkata and of pelletron at TIFR, Mumbai, are gratefully acknowledged for their very kind cooperation during the irradiation experiments. The author also thanks Mr Pradipta Kumar Das and Mr Kaushik Chatterjee for their help in the preparation of this manuscript.

#### REFERENCES

1. Siegel, R.W. Positron annihilation spectroscopy. *Annu. Rev. Mater. Sci.* 1980, **10**, 393-425.
2. Nambissan, P.M.G. & Sen, P. Positron annihilation studies on alpha-irradiated tungsten. *Solid State Commun.*, 1989, **71**, 1165-1673.
3. Mukherjee, P.; Nambissan, P.M.G.; Sen, P.; Barat, P. & Bandyopadhyay, S.K. Proton irradiation effects in Zr-1.0Nb-1.0Sn-0.1Fe probed by positron annihilation. *J. Nucl. Mater.*, 1999, **273**, 338-42.
4. Nambissan, P.M.G., Sen, P., & Viswanathan, B., Helium bubbles in molybdenum investigated by positron annihilation spectroscopy. *Rad. Eff. Def. Solids.* 1991, **116**, 125-35.
5. Maji, Sanjib.; Singh, Amarjeet. & Nambissan, P.M.G. Solid phase transition of overpressurised helium bubbles seen from positron annihilation studies. *Phys. Lett. A.*, 2001, **281**, 76-82.
6. Arya, A.S., & Nambissan, P.M.G. Positron annihilation spectroscopic studies of inert gas nanoclusters in metals (Unpublished).
7. Nambissan, P.M.G., Bhagwat, P.V., & Kurup, M.B. *J. Appl. Phys.*, 2007, **101**, 113526-6 pages.
8. Pandey, Brajesh.; Nambissan, P.M.G.; Mondal, N.N.; Bhagwat, P.V. & Verma, H.C.H.C. B<sup>5+</sup> ion-irradiation induced defects and their migration under annealing in Fe<sub>72</sub>Al<sub>28</sub> alloy studied by positron annihilation (Unpublished).
9. Olsen, J.V.; Kirkegaard, P.; Pedersen, N.J. & Eldrup, M. PALSfit : A new program for the evaluation of positron lifetime spectra. *Phys. Stat. Sol.*, 2007(c) **4**, 4004-4006.
10. Hautajarvi, P. & Corbel, C. (Eds.), Positron Spectroscopy of Solids Amsterdam: IOS Press, 1995. pp 491-532.
11. Krause-Rehberg, R. & Leipner, H.S. (Eds.) Positron Annihilation in Semiconductors-Defect Studies Springer, Berlin, 1999. pp. 1-126.
12. Farnum, D.J.; Sommer, W.F. & Inal, O.T. A study of defects produced in tungsten by 800 MeV protons using field ion microscopy. *J. Nucl. Mater.* 1984, **122** & **123**, 996-1001.
13. Maier, K.; Peo, M.; Saile, B.; Schaefer, H.E. & Seeger, A. High-temperature positron annihilation and vacancy formation in refractory metals. *Philos. Mag.* 1979, **A 40**, 701-728.
14. de Vries, J.; van Veen, A.; de Lima, A.P. & Lourens, W. Proceedings of the Seventh International Conference on Positron Annihilation. World Scientific, Singapore 1985, 470-472.
15. Nambissan, P.M.G., & Sen, P., Positron annihilation study of the annealing behaviour of alpha induced defects in tungsten. *Rad. Eff. Def. Solids*, 1992, **124**, 215-221.
16. Schultz, Peter J. & Lynn, K.G. Interaction of positron beams with surfaces, thin films and interfaces. *Rev. Mod. Phys.* 1988, **60**, 701-79.
17. Mukherjee, P.; Nambissan, P.M.G.; Sen, P. Barat, P.; Bandyopadhyay, S.K.; Chakravartty, J.K.; Wadekar, S.L.; Banerjee, S.; Chattopadhyay, S.K.; Chatterjee, S.K., & Mitra, M.K. The study of microstructural defects and mechanical properties in proton-irradiated Zr-1.0%Nb-1.0%Sn-0.1%Fe. *J. Nucl. Mater.* 2001, **297**, 341-44.
18. Subrahmanyam, V.S.; Nambissan, P.M.G. & Sen, P. Helium bubbles in tungsten studied by positron annihilation. *Solid St. Commun.* 1994, **89**, 523-27.
19. Subrahmanyam, V.S.; Nambissan, P.M.G. & Sen, P. Microstructural evolution of defects and the nucleation of helium bubbles in niobium studied by positron annihilation. *Rad. Eff. Def. Solids* 1994, **132**, 169-78.
20. Subrahmanyam, V.S.; Nambissan, P.M.G., & Sen, P. Thermal evolution of alpha induced defects and helium bubbles in tantalum studied by positron annihilation. *J. Phys. Chem. Solids* 1996, **57**, 319-323.
21. Singh, Amarjeet, Maji, Sanjib, & Nambissan, P.M.G. Helium dislocation interaction in aluminium. *J. Phys. :Condens. Matter*, 2001, **13**, 177-187.
22. Jensen, K.O., & Nieminen, R.M. Helium bubbles in metals: Molecular-dynamics simulation and positron states. *Phys. Rev.* 1987, **B 35**, 2087-090.
23. Jensen, K.O., & Nieminen, R.M. Noble-gas bubbles in metals: Molecular-dynamics simulation and positron states. *Phys. Rev.* 1987, **B 36**, 8219-232.
24. Trinkaus, H. Energetics and formation kinetics of helium bubbles in metals. *Radiat. Eff.* 1983, **78**, 189-211.
25. Mills, R.L.; Liebenberg, D.H. & Bronson, J.C. Equation of states and melting properties of <sup>4</sup>He from measurements to 20 kbar. *Phys. Rev.* 1980, **B 21**, 5137- 148.
26. de la Cruz, R.M.; Pareja, R.; Segura, A.; Munoz, V. & Chery, A. Temperature effects on the positron annihilation

- characteristics in III-VI layered semiconductors. *J. Phys. Condens. Matter.* 1993, **5**, 971-76.
27. Dannefaer, S.; Mascher, P. & Kerr, D. Monovacancy formation enthalpy in silicon. *Phys. Phys. Rev. Lett.* 1986, **56**, 2195-198.
  28. Throwe, J.; Leung, T.C.; Nielsen, B.; Huomo, H. & Lynn, K.G. Search for thermally generated monovacancies in silicon using monoenergetic positrons. *Phys. Rev.* 1989, **B 40**, 12037-040.
  29. Asoka-Kumar, P.; Alatalo, M.; Ghosh, V.J.; Kruseman, A.C.; Nielsen, B. & Lynn, K.G. Increased elemental specificity of positron annihilation spectra. *Phys. Rev. Lett.* 1996, **77**, 2097-100.
  30. Nagai, Y.; Nonaka, T.; Hasegawa, M.; Kobayashi, Y.; Wang, C.L.; Zheng, W. & Zhang, C. Direct evidence of positron trapping at polar groups in a polymer-blend system. *Phys. Rev.* 1999, **B 60**, 11863-1866.
  31. Donnelly, S.E., & Evans, J.H., (Eds.) *Fundamental aspects of inert gases in solids*, (Plenum, New York), 1991.
  32. Eldrup M. Positron studies of gases and gas bubbles in metals. *Mater. Sci. Forum* 1992, **105-110**, 229-48.
  33. Chen, Z.Q.; Maekawa, M.; Yamamoto, S.; Kawasuso, A., Yuan, X.I., Sekiguchi, T., Suzuki, R., Ohdaira, T. Evolution of voids in  $Al^{+}$ -implanted  $ZnO$  probed by a slow positron beam, *Phys. Rev.* 2004, **B 69**, 035210-10 pages.
  34. Brauer, G.; Anwand, W.; Skorupa, W.; Brandshetter, S. & Teichert, C. Characterization of  $6H-SiC$  surfaces after ion implantation and annealing using positron annihilation spectroscopy and atomic force microscopy. *J. Appl. Phys.* 2006, **99**, 023523-8 pages.
  35. Fujinami, M.; Tsuge, T. & Tanaka, K. Characterization of defects in self-ion implanted  $Si$  using positron annihilation spectroscopy and Rutherford backscattering spectroscopy. *J. Appl. Phys.* 1996, **79**, 9017-021.
  36. Hao, Xiaopeng.; Zhou, Chunlan, Yu, Runshang, Wang, Baoyi, & Wei Long, J. *Nanosci. Characterization of implantation induced defects in  $Si$ -implanted  $SiO_2$  film.* *J. Nanosci. Nanotech.*, 2008, **8**, 1350-354.
  37. Slugen, Vladimir, Krsjak, Vladimir, Petriska, Martin, Zeman, Andrej, & Miklos, Marek, Positron annihilation study of alloys for fission and fusion technology. *Phys. Stat. Sol* 2007 **C 4**, 3481-484.
  38. Uedono, A.; Hatton, N.; Oqura, N.; Kudo, J.; Nishikawa, N.; Ohdaira, T.; Suzuki, R. & Mikado, T. Characterizing metal-oxide semiconductor structures consisting of  $HfSiO_x$  as gate dielectrics using monoenergetic positron beams. *Jpn. J. Appl. Phys.* 2004, **43**, 1254-259.
  39. Gwilliam, R.M.; Knights, A.P.; Burrows, C.P. & Coleman, P.G. Room temperature evolution of vacancy-type damage created by 2 keV  $B^{+}$  implantation of  $Si$ . *J. Vac. Sci. Technol.* 2002, **B 20**, 427-30.
  40. Golonka, P.; Kluza, M.; Dryzek, J. & Banace, K. Application of positron annihilation spectroscopy and proton NMR relaxation to examine biological samples. *Mol. Phys. Rep.* 2000, **29**, 224-27.

#### Contributor



**Prof P.M.G. Nambissan** obtained his MSc (Physics) from University of Calicut in Kerala in 1986. He obtained his PhD from Institute of Nuclear Physics, Kolkata in 1991. He joined the faculty in 1993 after a brief stint as Research Associate. He now holds the position of Professor in the Nuclear and Atomic Physics Division of the institute. Presently, he is on deputation as Course Director to

Department of Nanoscience, Kannur University, Kerala. He is known for his contributions in the field of positron annihilation spectroscopy of condensed matter and nanomaterials. He has carried out extensive studies in metals and alloys, quasicrystals, high temperature superconductors, intermetallic compounds and nanomaterials. He had especially conducted research in the field of high-energy radiation effects in metals and alloys and has altogether published more than 80 papers in reputed international journals, in addition to about 60 papers in various national and international conferences. He has presented papers in conferences held in China, United States, Germany, Japan, Canada and Czech Republic. For two years, he also served as Editor of the Positron Annihilation Newsletter published quarterly.

